frontiers in Physics

ORIGINAL RESEARCH
published: 10 July 2020
doi: 10.3389/fphy.2020.00241

First Phantom-Based Quantitative Assessment of Scandium-44 Using a Commercial PET Device

Thiago V. M. Lima[1,2,3]*, *Silvano Gnesin*[2], *Egbert Nitzsche*[4], *Pablo G. Ortega*[5,6], *Cristina Müller*[7] and *Nicholas P. van der Meulen*[7,8]

[1] Radiation Protection Group, Aarau Cantonal Hospital (KSA) AG, Aarau, Switzerland, [2] Institute of Radiation Physics, Lausanne University Hospital, University of Lausanne, Lausanne, Switzerland, [3] Institute of Radiology and Nuclear Medicine, Cantonal Hospital of Lucerne (LUKS) AG, Lucerne, Switzerland, [4] Institute of Nuclear Medicine and PET, Aarau Cantonal Hospital (KSA) AG, Aarau, Switzerland, [5] Institute of Fundamental Physics and Mathematics (IUFFyM), Salamanca, Spain, [6] Fundamental Physics Department, University of Salamanca, Salamanca, Spain, [7] Center for Radiopharmaceutical Sciences ETH-PSI-USZ, Paul Scherrer Institute, Villigen, Switzerland, [8] Laboratory of Radiochemistry, Paul Scherrer Institute, Villigen, Switzerland

OPEN ACCESS

Edited by:
Ivo Rausch,
Medical University of Vienna, Austria

Reviewed by:
Terence Riauka,
University of Alberta, Canada
Simon Ferguson,
University of Alberta, Canada, in collaboration with reviewer TR
Andreas Renner,
Vienna General Hospital, Austria

***Correspondence:**
Thiago V. M. Lima
thiago.lima@luks.ch

Specialty section:
This article was submitted to Medical Physics and Imaging, a section of the journal Frontiers in Physics

Received: *15 December 2019*
Accepted: *03 June 2020*
Published: *10 July 2020*

Citation:
Lima TVM, Gnesin S, Nitzsche E, Ortega PG, Müller C and van der Meulen NP (2020) First Phantom-Based Quantitative Assessment of Scandium-44 Using a Commercial PET Device. Front. Phys. 8:241. doi: 10.3389/fphy.2020.00241

Scandium (Sc) is a promising candidate for theranostic applications due to the existence of radioisotopes suitable for both imaging and therapy. A "proof-of-concept" study regarding first-in-human use of ^{44}Sc for imaging metastatic neuroendocrine tumors was reported recently, however, quantitative assessment of ^{44}Sc-based PET images was not performed. The aim of this study was to evaluate quantitative capabilities of ^{44}Sc-PET using a commercial PET scanner. The NEMA/IEC body phantom with ^{44}Sc was acquired according to the local protocol used for whole-body oncological [^{18}F]FDG PET examinations. Additionally, we characterized the signal recovery (recovery coefficient—RC) according to the iteration number. For all reconstructions, pertinent image corrections (normalization, dead time, activity decay, random coincidence, and attenuation) were applied. Presently, ^{44}Sc scatter corrections are not optimized and could, thus, result in quantitative bias. To investigate the best option, the data were reconstructed using different available scatter corrections (relative -RelSC- and absolute -AbsSC-) and an additional prompt-gamma correction (PGC). System cross-calibration with the local dose calibrator (BG_{cal}) and image noise, expressed by the coefficient of variation (COV), were evaluated in the homogeneous background region (5 kBq/mL) of the phantom. Maximum (RC_{max}) and 50% threshold recovery coefficients, corrected for background (RC_{A50}), were measured for all spherical inserts (25 kBq/mL) of the phantom. Acceptable COV (<15%) was achievable with low iteration numbers (<3). BG_{cal} differences were low: mean BG_{cal} were 77.8, 81.3, and 86.7%, for RelSC, AbsSC, and PGC, respectively. RC values exceeded the present RC range recommended for [^{18}F]FDG procedures. Using the iterations to be evaluated, RC_{A50} ranged from 29.9 to 59.9% for the smallest lesion (spherical insert of 10 mm diameter) and from 45.5 to 80.3% (13 mm), 66.4 to 75.6% (17 mm), 71.7 to 75.7% (22 mm), 75.1 to 78.6% (28 mm), and 76.7 to 80.9% (37 mm) for the, respectively spherical inserts. The results of

this study show that clinical ^{44}Sc-PET imaging has the potential to provide signal recovery in lesions of different sizes comparable to current ^{18}F-PET standards. In order to improve the quantitative accuracy of ^{44}Sc PET, optimized corrections are still necessary and will be investigated further in future.

Keywords: PET imaging, quantification, ^{44}Sc, theranostic, scatter correction, prompt-gamma correction

1. INTRODUCTION

Clinical theranostic application of ^{68}Ga ($T_{1/2}$ = 68 min, $E\beta^+_{av}$ = 830 keV, I = 89%) and ^{177}Lu ($T_{1/2}$ = 6.65 d, $E\beta^-$ av = 134 keV, I = 100%; E_γ = 113 keV I = 6%, 208 keV I = 10%) is now common for PET imaging and targeted radionuclide therapy, respectively. The ^{68}Ga/^{177}Lu theranostic couple is used for labeling with somatostatin analogs (e.g., DOTATOC or DOTATATE) and, more recently, also for PSMA-targeting ligands (e.g., PSMA-11 and PSMA-617), thereby, enabling radiotheranostics of neuroendocrine and prostate cancer, respectively [1–4].

PET is currently regarded as a more sensitive technology than SPECT and provides images with superior spatial resolution and improved quantification [5]. The switch from ^{111}In-based SPECT imaging, such as ^{111}In-octreotide, to the use of ^{68}Ga for PET imaging, represents a cornerstone in nuclear medicine: [^{68}Ga]Ga-DOTATATE demonstrated significantly superior image quality and, hence, outperformed ^{111}In-octreotide in both diagnostic accuracy and impact on treatment decisions [6].

^{68}Ga is obtained from a ^{68}Ge/^{68}Ga-generator system, which can be conveniently placed in a radiopharmacy at any hospital. The availability of ^{68}Ga is, however, restricted with regard to activity that can be eluted for radiopharmaceutical preparation, while the generator itself is also costly. A drawback of using ^{68}Ga, however, is its short half-life of only 68 min (compared to 2.81 d for ^{111}In), which does not allow scanning at late time points after injection nor transportation of ^{68}Ga-based radiopharmaceuticals over longer distances (when a ^{68}Ge/^{68}Ga generator is not present on site). Optimally, the physical half-life is identical to the biological half-life and ^{44}Sc can be used with targeting agents that are retained longer in the body. As an example, ^{44}Sc may be viable in the use of albumin-binding radiopharmaceuticals, which have longer circulation time [7]. Finally, it remains to be mentioned that ^{68}Ga has a different coordination chemistry compared to ^{177}Lu, therefore, ^{68}Ga results in different chelator-radiometal complexes and, hence, chemically unequal radiopharmaceuticals. This may result in different *in vivo* uptake patterns for both diagnostic and therapeutic radioligands [8–10].

Several years ago, ^{44}Sc was proposed as an alternative PET nuclide [11, 12]. The physical decay properties [13] of ^{44}Sc ($T_{1/2}$ = 4.04 h, average $E\beta^+$ = 632 keV, I = 94%) are attractive to address the shortcomings of ^{68}Ga mentioned above. It decays with an almost four-fold longer half-life than ^{68}Ga [13] by emitting relatively low energy β^+-particles that enables the acquisition of PET images with a spatial resolution equal or even superior to that achievable with ^{68}Ga [14]. The coordination chemistry allows the preparation of ^{44}Sc-radioconjugates using a DOTA-chelator in analogy with ^{177}Lu-labeling [9]. Preclinical experiments in mice showed almost identical distribution patterns for ^{44}Sc- and ^{177}Lu-labeled ligands [10, 11]. Consequently, ^{44}Sc may be adopted as a more favorable diagnostic match to ^{177}Lu than ^{68}Ga. In future, ^{47}Sc ($T_{1/2}$ = 3.35 d, average $E\beta^-$ = 162 keV, I = 100%; $E\gamma$ = 159 keV I = 68%) can be employed as a therapeutic match to provide chemically-identical ^{44}Sc/^{47}Sc-based radiopharmaceuticals for radiotheranostic applications [15–17]. A possible addition to the scandium radioisotope family, due to its theoretically more favorable characteristics for PET imaging, is ^{43}Sc. [18]. Although it provides possible advantages in terms of gamma emission, it is currently more challenging to produce in terms of yield, as well as cost [19, 20].

Rösch and co-workers performed preliminary studies using ^{44}Sc obtained from a ^{44}Ti/^{44}Sc generator system [21]. First PET images of a patient administered with [^{44}Sc]Sc-DOTATOC looked promising, where somatostatin-receptor-positive liver metastases were imaged and visible 18 h after administration of 37 MBq [22]. It was later proposed to produce ^{44}Sc at a cyclotron using natural Ca targets, in an attempt to simplify production and increase yield [23, 24]. At PSI, it was demonstrated for the first time that ^{44}Sc can also be produced in high quantities and good quality when using enriched ^{44}Ca targets [11, 25]. In recent years, the production was constantly improved, currently enabling the preparation of up to 5 GBq ^{44}Sc with small quantities of target material. This production method may be translated to a conventional medical cyclotron commonly installed in PET centers. Subsequently, the application of cyclotron-produced ^{44}Sc in two patients with neuroendocrine neoplasms, receiving a diagnostic administration of [^{44}Sc]Sc-DOTATOC at Zentralklinik Bad Berka (Germany), was reported [26]. First-in-man studies with [^{44}Sc] Sc-PSMA-617, using generator-produced ^{44}Sc, were reported recently in the literature, underlining the excellent features of ^{44}Sc in a clinical setting [27].

Despite the reported clinical advantages of ^{44}Sc, its use could potentially be restricted by the currently limited quantification capability of clinical devices. The first reported human study using ^{44}Sc [26] indicated that absolute quantification was not available, but the authors did not discuss this limitation further. Other studies on the use of non-pure positron emitters started evaluating this limitation. In particular, the importance of adopting adapted and optimized corrections in the acquisition and reconstruction process, in achieving quantitative imaging in clinical setups, was highlighted. As an example, the work by Armstrong et al. [28] addressed the impact of prompt-gamma coincidence inducing quantitative artifacts and underlined the important role of specific corrections in absolute quantification using ^{82}Rb cardiac imaging. The study by Lubberink and Herzog

[29] reviewed different optimization strategies for improving quantification of ^{124}I and ^{86}Y, including effects from scatter and prompt-gamma corrections.

The aim of this paper was to evaluate the quantification capabilities of ^{44}Sc in a clinically-relevant phantom configuration study performed with a commercial PET scanner.

2. MATERIALS AND METHODS

The experimental design presented in this work included (a) image acquisitions of a NEMA/IEC NU2 phantom (see sections 2.1, 2.2) and (b) the subsequent data analysis (see sections 2.3, 2.4). The phantom was scanned under clinically-relevant conditions at the Aarau Cantonal Hospital (KSA) using a mCT Biograph PET-CT (Siemens Healthineers AG) [30]. ^{44}Sc was produced via the ^{44}Ca(p,n)^{44}Sc nuclear reaction at Injector 2 cyclotron facility at Paul Scherrer Institute (PSI), Switzerland, as previously reported [25, 26].

The reference activity received from PSI was used to perform a cross calibration of the local dose calibrator (Veenstra Instruments, Joure, Netherlands VDC-405 with ionization chamber VIK-202). At PSI, the nuclide content in the irradiated targets was identified and quantified by γ-ray spectrometry using an N-type high-purity germanium (HPGe) coaxial detector (EURISYS MESURES, France) and the Ortec InterWinner 5.0 software. A dose calibrator (ISOMED 2010, Nuclear-Medizintechnik Dresden GmbH, Germany) was employed for the quantitative determination of ^{44}Sc activity [20]. The reference activity was measured at the end of chemical separation and the time noted, before packing and transportation. This reference activity and time, on its original vial, was used to cross calibrate the local dose calibrator by modifying the isotope settings (factor and scale) to match this reference activity. The factor obtained was then used for all dispensing syringe activities. The activities obtained for various settings, along with the setting chosen for ^{44}Sc, are listed in **Table 1**. All measurements were decay-corrected to the reference activity. These values were then used to estimate the injected activity (IA) used to fill the main phantom volume (background volume) and the included spherical inserts, representing lesions. The ^{44}Sc cross-calibrated factor (presented in **Table 1**) was then used for all activity dispensing.

TABLE 1 | Reference activity and employed factors for determination of the local dose calibrator factor for ^{44}Sc measurements.

Radionuclide	Setting (Factor and scale)	Measurement (GBq)
Ga-68	751 scale 1	2.116
F-18	765 scale 1	1.401
Co-60	889 scale 1	0.392
Sc-44	760 scale 0.56	0.594
Reference activity		0.595

All measurements were decay-corrected to the reference time provided by PSI. The factor is constrained to a given range (0–900) and for some radionuclides, a scale different than 1 is also needed.

2.1. Phantom Preparation

The NEMA/IEC NU2 phantom (PTW, Freiburg, Germany) used in this study enabled the characterization of image quality and quantitative signal recovery in the main background phantom volume and in spherical structures of different size potentially affected by partial-volume-effect (PVE). The NEMA/IEC phantom is composed of a main volume (background) of 9.5 L that mimics the human abdominal shape. The phantom includes a set of hollow-glass-sphere inserts of variable diameters: 10, 13, 17, 22, 18, and 37 mm, respectively. In addition, a lung insert (5-mm-diameter and 16-cm-long cylinder filled with plastic material to reproduce the lung density of 0.3 g/mL) was placed in the center of the phantom to simulate lung tissue attenuation. The phantom was filled with a background activity concentration of 5 kBq/mL and a five-fold higher activity concentration (25 kBq/mL) in the spherical inserts. The activity concentration and background ratio used was chosen to mimic the average hepatic activity concentration measured in patients when using [^{18}F]FDG oncological PET 1 h after administration of a mass-activity of 3.5 MBq/kg. This corresponded to the recommended dose reference level in Switzerland at the time of this study for this specific examination [31]. The adopted experimental setup allowed comparison with previously published results obtained with [^{18}F]FDG for the same device [31].

2.2. PET Acquisition and Reconstructions

The Siemens mCT PET, utilized for the phantom acquisitions performed in this work, consists of 4 rings, with 48 detector blocks in each ring and lutetium oxyorthosilicate (LSO) crystals, a PET field-of-view (FOV) of 22.1 cm and transaxial FOV of 70 cm. The detector ring diameter is 84.2 cm, the reported time coincidence window is 4.1 ns, system time-of-flight (TOF) 540 ps, and energy window 435–650 keV. The phantom was placed on the PET bed to have the equatorial plane of the spherical inserts at the center of the device FOV, where the system sensitivity is expected to be at its maximum. A single-bed, step-and-shoot, 300 s, list-mode (LM) acquisition was performed. The LM data were reconstructed according to the local clinic protocol used for whole-body oncological [^{18}F]FDG PET examinations, with acquisition time of 150 s per bed position. For the acquisition, the vendor specific setup for the radionuclide ^{44}Sc was selected, taking a positron fraction of 0.9427 and half-life of 3.97 h into consideration.

Supplementary reconstructions were performed, in addition to the local clinical protocol, by varying the number of iterations from 1 to 10 with 21 fixed subsets. This was done in order to characterize the convergence of the signal recovery in background areas, the spheres, and the lung. Reconstructions were performed using the TOF information and the point-spread function correction implemented in the vendor-based iterative reconstruction algorithm (TrueX + TOF - ultraHD-PET).

2.3. Data Analysis

2.3.1. PET vs. Dose Calibrator Activity Cross-Calibration (BG_{cal})

The PET to local dose calibrator activity cross calibration (BG_{cal}) was tested by calculating the ratio between the measured PET

signal ($\overline{A}_{c,bg}$) and the expected average activity concentration ($A_{c,bg}$) evaluated in the homogeneous background regions of the phantom:

$$BG_{cal} = \frac{\overline{A}_{c,bg}}{A_{c,bg}} \quad (1)$$

$\overline{A}_{c,bg}$ was measured in four cubic regions of interest (40 mm per side) placed in the homogeneous background region of the phantom which surrounded the spheres. When using [^{18}F]FDG, a deviation <0.1 from the ideal BG_{cal} =1 is regarded as acceptable.

2.3.2. Noise

The image noise was evaluated by the coefficient of variation (COV), which is the ratio between the standard deviation and the average activity concentration measured in same cubic volumes of interest (VOIs) of the phantom background described above for the cross-calibration assessment:

$$COV(\%) = \frac{SD_{bg}}{\overline{A}_{bg}} * 100 \quad (2)$$

The background signal-to-noise ratio (SNR) is the reciprocal of the COV. A COV $\leq$15% (background SNR $\geq$ 6.7) was considered as an acceptable noise level for clinical image interpretation, as suggested in the EARL procedure [32]. Although this value is somehow arbitrary, it has already been used as a reference value in previously-published works [33–35], which enables a term of comparison for image quality assessments.

2.3.3. Average Residual Lung Error

A cylindrical VOI 30 mm in diameter and 120 mm in length was included in the lung insert. The average residual lung error (in %) was obtaining by:

$$\overline{LE}(\%) = \frac{\overline{L}_c}{\overline{A}_{c,bg}} * 100 \quad (3)$$

where $\overline{L}_c$ is mean counts in the lung region and $\overline{A}_{c,bg}$ is the average activity concentration in the background region.

2.3.4. Recovery Coefficient

A VOI, with a side of 50 mm in length, was centered on each of the six spheres of the phantom. For each spherical insert (j = 1...6) the maximum and the background-adapted recovery coefficients (RC) were obtained as follows:

$$RC_{j,max}(\%) = \frac{a_{c,sph,j,max}}{A_{c,sph}} * 100 \quad (4)$$

$$RC_{j,A50}(\%) = \frac{a_{c,sph,j,A50}}{A_{c,sph}} * 100 \quad (5)$$

where $A_{c,sph}$ is the expected activity concentration in the spheres, $a_{c,sph,j,max}$ is the measured maximum voxel value (in terms of activity concentration) for a given spherical insert. $a_{c,sph,j,A50}$ is, for each considered spherical insert, the average voxel value in a VOI, defined by a 3D-iso-contour adapted for background [as defined in [32]] as recommended by the EANM Guidelines for [^{18}F]FDG tumor PET imaging [35]. The numerator of Equation (5), for a given sphere *j*, is the average activity concentration computed from voxels in the $VOI_{sph,j,A50}$. The $VOI_{sph,j,A50}$ includes all voxels with activity concentration $\geq$ $(acj, max + \overline{A}_{c,bg})/2$, where acj, max is a maximum activity concentration assumed in the hot sphere *j*. RC calculations were performed using a Matlab script.

Calculated RC_{max} and RC_{A50} values were compared with reference values provided by the EANM/EARL accreditation protocol [36].

2.3.5. Evaluation of Available Scatter and Prompt Gamma Corrections

Pertinent image corrections (normalization, dead time, activity decay, random coincidence, and attenuation) were applied to all reconstructions performed. A known limitation that applies to radionuclides not routinely used in clinical studies (particularly if they are non-pure positron emitters) exists on the applied system corrections that were optimized for the ^{18}F PET setting and not, in this case, for the ^{44}Sc.

For this reason, along with the clinical corrections, all possible scatter corrections available in the iterative reconstruction algorithm (relative and absolute scatter corrections) were tested, thereby, producing a set of dedicated reconstructions [37]. Additionally, we applied the available prompt-gamma correction (PGC) [38] to evaluate the contributions of high-energy γ-emissions of ^{44}Sc to the quantitative accuracy of reconstructed PET images.

Evaluated scatter methods differ mainly on the procedure used to account for scatter events at the sinogram level [39]. The absolute scatter correction relies on the single scatter estimation (SSS) algorithm [37], which estimates the scatter distribution produced by a single scatter event and integrates this contribution over the whole acquired FOV volume. The relative scatter correction, on the other hand, scales the SSS (plane-by-plane) to the net trues based on a scaling mask computed outside the emission object. The volume covered by the emission object is known from the transmission sinogram obtained from the CT acquisition. Based on the CT information, the emitting object and the outside region masks are generated and applied to correct the emission object sinogram. Similar to the methodology, the PGC is estimated by the single event rates. The PG model is combined with a scatter sinogram estimated by the SSS algorithm, and the total background model is scaled to fit the tails of the measured data [38]. Additionally, further contributions from PGC can be addressed as described by Armstrong et al. [28] and Lubberink and Herzog [29].

Statistical analyses were performed with Python Scipy statistical module using the Wilcoxon signed rank test. Additionally, differences between the obtained COV and BG_{cal} were calculated between the reconstructions obtained in

comparison to the original/reference reconstruction (absolute scatter correction with PSF and TOF).

$$Difference(\%) = \frac{S_{refrecon} - S_{testedrecon}}{S_{refrecon}} * 100 \quad (6)$$

3. RESULTS

The effect of the iteration number on the noise (COV), average residual lung error and the BG calibration obtained in the tested reconstructed images are presented in **Figure 1**.

Noise level within acceptable ranges (15% was used as level of comparison to [^{18}F]FDG [32]) is achievable with low iteration numbers (iterations $\leq$3 when subsets = 21) and increases as the iteration number increases for all evaluated corrections.

Figure 1 also shows the effect of the used scatter correction (SC) model (absolute vs. relative) on the obtained COV and background calibration values. The main observed result is the reduced background calibration level obtained for reconstructions employing the relative scatter in comparison to other evaluated corrections. The BG calibration values did not vary with the tested number of iterations, averaged at 0.81 ($\pm$ 0.01), 0.78 ($\pm$ 0.01), and 0.87 ($\pm$ 0.01), respectively for the absolute scatter correction, relative scatter correction and PGC. With the results obtained with PGC, it was observed that the BG calibration improved in relation to the original (absolute scatter correction and no PGC), and the previously-evaluated relative scatter. Both differences were statistically significant with p-value < 0.001. **Figure 1** also shows the average residual lung error obtained.

Additionally, **Figure 1** shows that the average residual lung error reduces with the increase of iteration number and a small difference ($\leq$ 4%) was observed between the evaluated corrections.

Figure 2 shows scatter corrections and PGC profiles obtained on the acquired sinogram. All plots discriminate the contributions from the emission and scatter estimate sinograms and the subtraction mask used for scatter modeling without (B–relative scatter) and with PGC (C), respectively. Differences depends on the size of the applied scatter mask (blue dashed line) and, subsequently, the extrapolation of events obtained outside the central part of the sinogram and the scaled scatter estimate (green line). Noticeably, the initial scatter sinogram (SSS) is further overestimated with the relative scatter by using the wider mask, the PGC is able to improve the applied correction. The effect of this was seen in the BG calibration in **Figure 1**.

Lastly, recovery coefficients were evaluated for all reconstructed PET images, depending on the applied correction (PGC, no PGC with absolute scatter correction and no PGC with relative scatter correction), as a function of the number of iterations. **Figure 3** shows the obtained RC_{A50} and RC_{max} for all spherical inserts of the phantom across the evaluated reconstructions.

4. DISCUSSION

In this work, the quantitative capabilities of a clinical PET/CT device using ^{44}Sc in a well-characterized phantom-based setup was investigated for the first time. Quantitative ^{44}Sc PET/CT

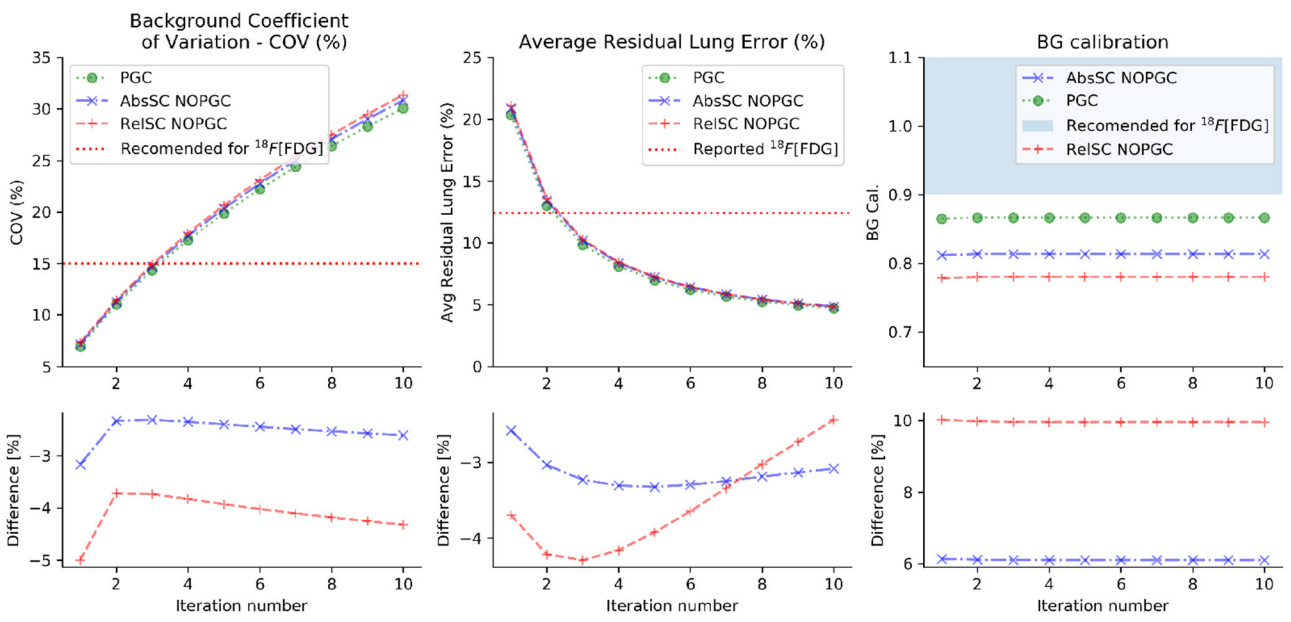

FIGURE 1 | Noise level (COV), average residual lung error and local cross-calibration for ^{44}Sc obtained as a function of the tested iteration numbers for the different evaluated corrections (absolute scatter correction, relative scatter correction and PGC). The differences (in %) between the absolute or relative scatter correction in respect to the PGC is displayed in the lower plots. All reconstructions were performed (similarly to clinical ^{18}F PET setup) with absolute scatter correction, PSF and TOF.

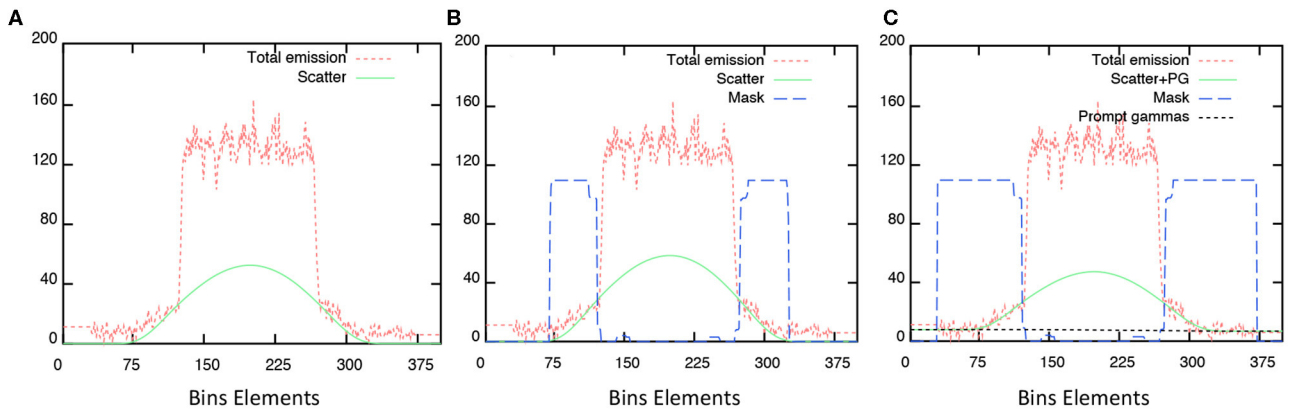

FIGURE 2 | Profiles obtained from measured sinograms superimposed with the estimated scatter corrections applied: **(A)** absolute scatter correction; **(B)** relative scatter correction, and; **(C)** with PGC.

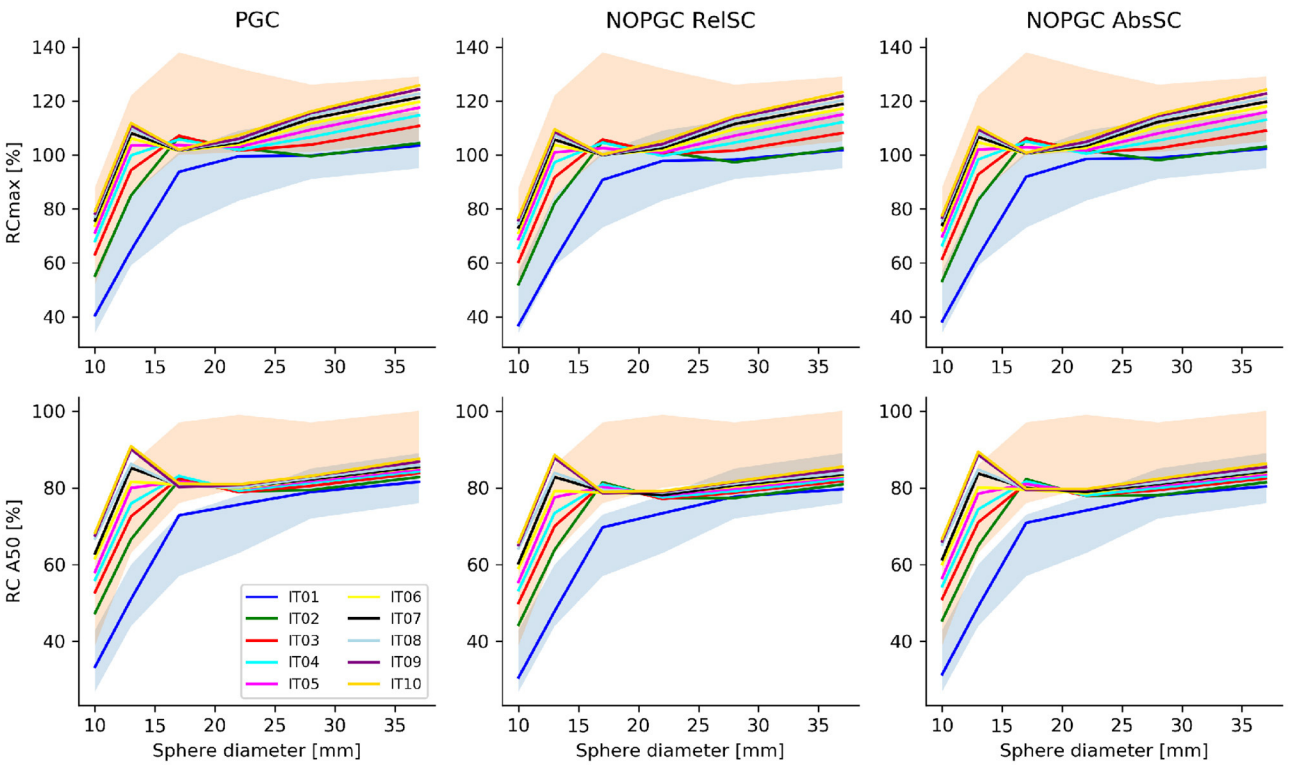

FIGURE 3 | RC_{max} and RC_{A50} obtained as a function of the sphere size for the tested number of iterations (from 1 to 10, for a fixed number of 21 subsets) and for the different scatter/PGC tested corrections. The range of RC values recommended in the EANM/EARL accreditation procedure for [^{18}F]FDG PET is indicated in blue. The RC range of values proposed by Kaelep et al. [34] is within the shaded red area.

performances were compared with reference performance levels known for the well-established ^{18}F PET imaging. We reported quantitative accuracy (BG calibration) and noise level (COV) assessed in a PVE-free background volume (the main volume of the NEMA/IEC NU2 phantom) and recovery coefficients obtained in spherical inserts of different size. In particular, we investigated the impact of different scatter models and PGC available in the vendor-based iterative reconstruction algorithm.

With regard to the noise, the results presented showed that, with clinically relevant activity concentrations, scan duration and reconstruction setups, noise levels below 15% can be achieved for a low number of iterations. These results, in terms of noise levels and, additionally, to the average residual lung error, are comparable to published results obtained with [^{18}F]FDG [31, 40] in similar clinical configurations for the same device.

Of note, it was found, according to the local dose calibrator cross-calibration, that the background quantitative signal was significantly below the acceptable performance levels considered for commonly-used PET radionuclides (for instance, BG_{cal} out of the 1 ± 0.1 range defined as acceptable for ^{18}F; **Figure 1**). In a recent publication [41], the authors reported the results form a survey across Dutch hospitals (8 centers, 13 different PET/CT), describing performance standard achievable in quantitative PET for both ^{68}Ga and ^{18}F. In particular, they found a system cross-calibration within 15% deviation in all tested devices and within 10% in 10 of 13 devices. We previously reported a background cross calibration of <5% deviation using ^{18}F for the mCT PET/CT system used in this work [31].

The low level of the measured background activity concentration could possibly be attributed to the specificity of the ^{44}Sc decay (non-pure positron emission with associated high-energy prompt-gamma emission) which would significantly bias quantitative PET images in absence of optimized scatter and prompt-gamma corrections.

We initially considered the measured low level of BG calibration potentially ascribed to a non-appropriate scatter correction which, in the specific case, acted as an over-correction that resulted in an artificial depletion of the signal from the background volume. Further reconstructions were, therefore, performed using the scatter correction methods (relative and absolute) available from the vendor-based reconstruction algorithm implemented in the tested commercial PET/CT device.

Based on the results presented in this study, the available PGC improved the absolute quantitative accuracy of ^{44}Sc PET, in agreement with results reported by Armstrong et al. [28] and Lubberink and Herzog [29] for other PET radionuclides. The impact of this correction is visible in **Figure 2**, where the overall scatter contribution was reduced, subsequently, improving the quantitative accuracy of the recovered activity concentration in the phantom background (**Figure 1**). The PGC fraction, although small, was not negligible: the difference between PGC reconstruction and non-PGC reconstructions was significant in terms of background calibration (p-values < 0.01 for non-PGC absolute and relative scatter corrections, respectively). Although the application of the PGC resulted in an improved quantitative accuracy, this was still well below accuracy levels obtained for ^{18}F and ^{68}Ga, which could indicate that further optimization could be performed. The average residual lung error was also found to be close to the reported ^{18}F values for a similar device [40].

According to data presented in **Figure 3**, we observed that, even in the presence of a sub-optimal signal recovery, the uniform background, the signal recovery for spherical inserts with a diameter of <20 mm exceeded the reference range on values provided by the EANM/EARL recommendation [33]. It has been observed that RC values significantly higher than

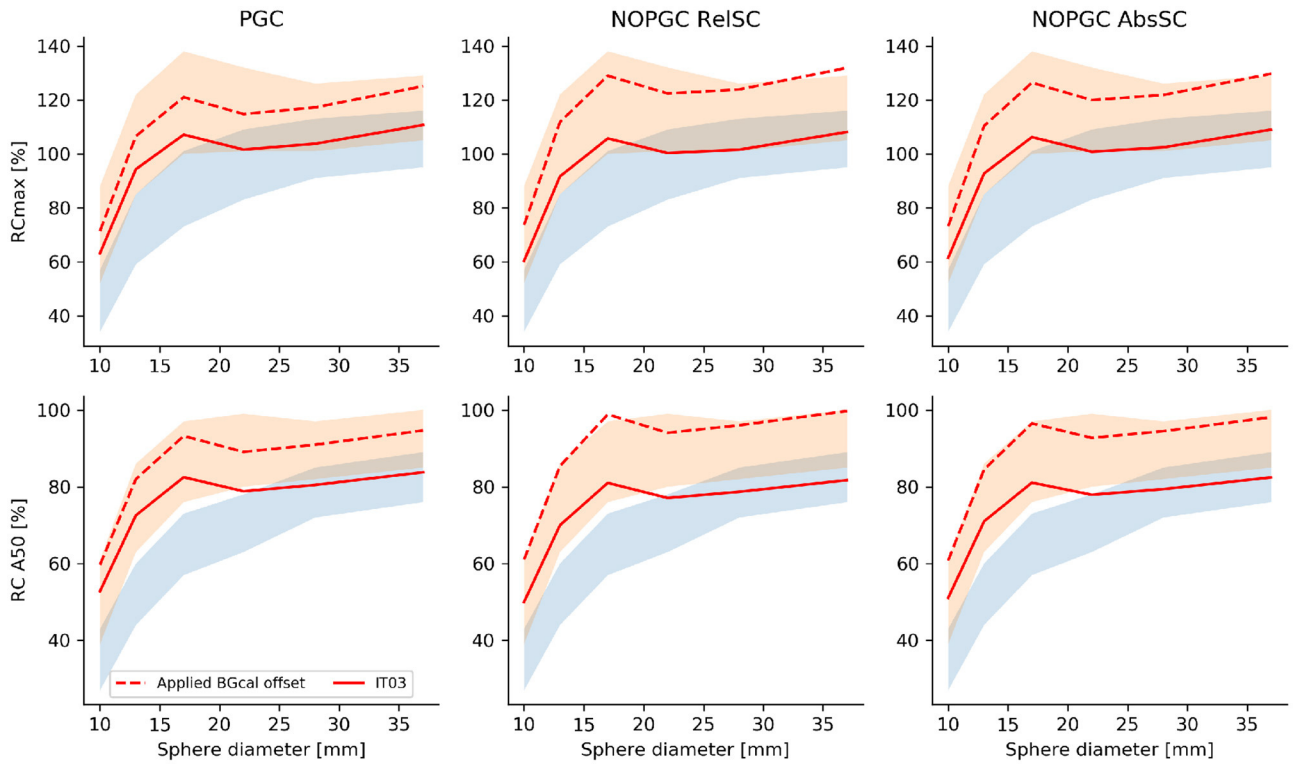

FIGURE 4 | RC_{max} and RC_{A50} obtained as a function of the sphere size for the optimal reconstruction (3 iterations and 21 subsets) and for the different scatter/PGC tested corrections (red full lines). Additionally we presented corrected RCs obtained by compensating for the low BGcal measured in the PET reconstructions to match a BGcal offset of 1 (red dashed lines). The EANM/EARL reference range of values is within the blue shaded area, the RC range of values proposed by Kaelep et al. [34] is within the red shaded area.

EANM/EARL reference values are commonly obtained when iterative reconstruction using both PSF and TOF information are used [34]. For this reason, the recommended range of RC values recommended by Kaalep et al. was also considered (red shaded area in **Figure 3**). Recovery coefficients (RC_{A50}) were [31.5:66.8], [45.5:80.3], [66.4:75.6], [71.7:75.7], [75.1:78:6], and [76.7:80.9] for the 10, 13, 17, 22, 28, and 37 mm spherical inserts, respectively, on the reconstruction with absolute scatter and no PGC; confirming a quantitative signal recovery in the lower range of the values provided by Kaelep et al. [34]. To compensate for the quantitative offset caused by the background calibration (BGcal < 1), we presented, for the optimal reconstruction setup (3 iterations), corrected RCs obtained by scaling up the measured RCs presented in **Figure 3** by the respective BGcal offset compared to BGcal $= 1$ adopted in the NEMA approach. Corrected RCs are shown in **Figure 4** and falls well within the range of values proposed by Kealep et al. [34], for PET reconstructions adopting TOF and PSF information. This observation further supports the hypothesis that achievable signal recovery in ^{44}Sc PET is comparable to that achievable with ^{18}F and ^{68}Ga.

4.1. Limitations

This paper focused on the quantitative accuracy performances of a clinical PET scanner to quantify ^{44}Sc. The present study does not investigate possible sources of quantitative bias, such as the effect of the positron range, in addition to the configured branching factor and its impact on quantification of ^{44}Sc.

A possible explanation for the measured low level of background calibration could arise from the methodology adopted to determine the ^{44}Sc activity. In this work the cross calibration relied on a reference activity value provided by PSI. The obtained factor was then used for all dispensing syringe activities. A different approach described in the literature [12, 42] defines the absolute ^{44}Sc activity as the measured activity using the ^{18}F dose calibrator settings multiplied by a factor (0.7). Although this approach has been tested, we found that this doesn't correlate to our findings. By using this approach, we would have received 980.7 MBq at the reference time although the dispatched activity was 595.0 MBq. As a result, this approach was not further considered.

Phantom preparation and data analysis applied in our study differs in some points from the EARL (or NEMA) procedures (for instance, the lesion-to-background activity concentration ratio) and might impair a full comparability of results obtained with the cited procedures. Nevertheless, we consider that comparing our results with EARL proposed reference values (for the COV and RCs) would still be meaningful.

5. CONCLUSION

In this work, we evaluated the capability of a commercial PET/CT device to produce accurate quantitative imaging with ^{44}Sc, for the first time. We performed dedicated ^{44}Sc PET acquisitions using a controlled and clinical relevant phantom-based setup. Quantitative ^{44}Sc PET performances, in terms of quantitative accuracy and noise levels, were shown to be comparable to that achieved in ^{18}F PET. In particular, this study outlined that available scatter and prompt-gamma corrections plays an important role in ^{44}Sc PET quantification. In view of a broader clinical application of ^{44}Sc-based radiopharmaceuticals, it is essential to further improve and optimize these features.

DATA AVAILABILITY STATEMENT

The datasets generated for this study are available on request to the corresponding author.

AUTHOR CONTRIBUTIONS

All listed authors made substantial contributions in all four of the following categories.

- Substantial contributions to the conception or design of the work, or the acquisition, analysis, or interpretation of data for the work.
- Drafting the work or revising it critically for important intellectual content.
- Provide approval for publication of the content.
- Agree to be accountable for all aspects of the work in ensuring that questions related to the accuracy or integrity of any part of the work are appropriately investigated and resolved.

More specifically, TL, SG, EN, CM, and NM coordinated the project and set up the framework. NM and CM coordinated the ^{44}Sc production. TL and SG performed the phantom preparation, measurements, and analysis. PO contributed to the data analysis.

FUNDING

CM and NM were supported by the Swiss National Science Foundation (IZLIZ3-156800).

ACKNOWLEDGMENTS

The authors thank Alexander Sommerhalder and Walter Hirzel, Radionuclide Production and Maintenance group at the Center for Radiopharmaceutical Sciences, PSI, for technical assistance toward the production of ^{44}Sc, as well as the people responsible for radioactive transports. Additionally, the authors would like to thank Dr. M. Conti and Dr. H. Bal from Siemens Healthineers AG for their support and discussions on the current and research corrections.

REFERENCES

1. Afshar-Oromieh A, Holland-Letz T, Giesel FL, Kratochwil C, Mier W, Haufe S, et al. Diagnostic performance of ^{68}Ga-PSMA-11 (HBED-CC) PET/CT in patients with recurrent prostate cancer: evaluation in 1007 patients. *Eur J Nucl Med Mol Imaging*. (2017) **44**:1258–68. doi: 10.1007/s00259-017-3711-7
2. Fendler WP, Rahbar K, Herrmann K, Kratochwil C, Eiber M. ^{177}Lu-PSMA radioligand therapy for prostate cancer. *J Nucl Med*. (2017) **58**:1196–200. doi: 10.2967/jnumed.117.191023
3. Haug AR, Cindea-Drimus R, Auernhammer CJ, Reincke M, Wängler B, Uebleis C, et al. The role of ^{68}Ga-DOTATATE PET/CT in suspected neuroendocrine tumors. *J Nucl Med*. (2012) **53**:1686–92. doi: 10.2967/jnumed.111.101675
4. Kwekkeboom DJ, Kam BL, Van Essen M, Teunissen JJ, van Eijck CH, Valkema R, et al. Somatostatin receptor-based imaging and therapy of gastroenteropancreatic neuroendocrine tumors. *Endocr Relat Cancer*. (2010) **17**:R53–73. doi: 10.1677/ERC-09-0078
5. Rahmim A, Zaidi H. PET versus SPECT: strengths, limitations and challenges. *Nucl Med Commun*. (2008) **29**:193–207. doi: 10.1097/MNM.0b013e3282f3a515
6. Deppen SA, Blume J, Bobbey AJ, Shah C, Graham MM, Lee P, et al. ^{68}Ga-DOTATATE compared with 111In-DTPA-octreotide and conventional imaging for pulmonary and gastroenteropancreatic neuroendocrine tumors: a systematic review and meta-analysis. *J Nucl Med*. (2016) **57**:872–8. doi: 10.2967/jnumed.115.165803
7. Lau J, Jacobson O, Niu G, Lin KS, Bénard F, Chen X. Bench to bedside: albumin binders for improved cancer radioligand therapies. *Bioconj Chem*. (2019) **30**:487–502. doi: 10.1021/acs.bioconjchem.8b00919
8. Sainz-Esteban A, Prasad V, Schuchardt C, Zachert C, Carril JM, Baum RP. Comparison of sequential planar 177 Lu-DOTA-TATE dosimetry scans with ^{68}Ga-DOTA-TATE PET/CT images in patients with metastasized neuroendocrine tumours undergoing peptide receptor radionuclide therapy. *Eur J Nucl Med Mol Imaging*. (2012) **39**:501–11. doi: 10.1007/s00259-011-2003-x
9. Domnanich KA, Müller C, Farkas R, Schmid RM, Ponsard B, Schibli R, et al. 44 SC for labeling of DOTA-and NODAGA-functionalized peptides: preclinical *in vitro* and *in vivo* investigations. *EJNMMI Radiopharm Chem*. (2017) **1**:8. doi: 10.1186/s41181-016-0013-5
10. Umbricht CA, Benešová M, Schmid RM, Türler A, Schibli R, van der Meulen NP, et al. ^{44}Sc-PSMA-617 for radiotheragnostics in tandem with 177 Lu-PSMA-617–preclinical investigations in comparison with 68 Ga-PSMA-11 and 68 Ga-PSMA-617. *EJNMMI Res*. (2017) **7**:9. doi: 10.1186/s13550-017-0257-4
11. Müller C, Bunka M, Reber J, Fischer C, Zhernosekov K, Türler A, et al. Promises of cyclotron-produced ^{44}Sc as a diagnostic match for trivalent β-emitters: *in vitro* and *in vivo* study of a ^{44}Sc-DOTA-folate conjugate. *J Nucl Med*. (2013) **54**:2168–74. doi: 10.2967/jnumed.113.123810
12. Roesch F. Scandium-44: benefits of a long-lived PET radionuclide available from the 44Ti/44Sc generator system. *Curr Radiopharm*. (2012) **5**:187–201. doi: 10.2174/1874471011205030187
13. Garcia-Torano E, Peyres V, Roteta M, Sanchez-Cabezudo A, Romero E, Ortega AM. Standardisation and precise determination of the half-life of ^{44}Sc. *Appl Radiat Isotopes*. (2016) **109**:314–8. doi: 10.1016/j.apradiso.2015.12.007
14. Bunka M, Müller C, Vermeulen C, Haller S, Türler A, Schibli R, et al. Imaging quality of ^{44}Sc in comparison with five other PET radionuclides using Derenzo phantoms and preclinical PET. *Appl Radiat Isotopes*. (2016) **110**:129–33. doi: 10.1016/j.apradiso.2016.01.006
15. Müller C, Bunka M, Haller S, Köster U, Groehn V, Bernhardt P, et al. Promising prospects for ^{44}Sc-/^{47}Sc-based theragnostics: application of ^{47}Sc for radionuclide tumor therapy in mice. *J Nucl Med*. (2014) **55**:1658–64. doi: 10.2967/jnumed.114.141614
16. Siwowska K, Guzik P, Domnanich KA, Monné Rodríguez JM, Bernhardt P, Ponsard B, et al. Therapeutic potential of ^{47}Sc in comparison to ^{177}Lu and 90Y: preclinical investigations. *Pharmaceutics*. (2019) **11**:424. doi: 10.3390/pharmaceutics11080424
17. Domnanich KA, Müller C, Benešová M, Dressler R, Haller S, Köster U, et al. ^{47}Sc as useful β–emitter for the radiotheragnostic paradigm: a comparative study of feasible production routes. *EJNMMI Radiopharm Chem*. (2017) **2**:5. doi: 10.1186/s41181-017-0024-x
18. Chaple IF, Lapi SE. Production and use of the first-row transition metal PET radionuclides 43, 44Sc, 52Mn, and 45Ti. *J Nucl Med*. (2018) **59**:1655–9. doi: 10.2967/jnumed.118.213264
19. Carzaniga TS, Auger M, Braccini S, Bunka M, Ereditato A, Nesteruk KP, et al. Measurement of ^{43}Sc and ^{44}Sc production cross-section with an 18 MeV medical PET cyclotron. *Appl Radiat Isotopes*. (2017) **129**:96–102. doi: 10.1016/j.apradiso.2017.08.013
20. Domnanich KA, Eichler R, Müller C, Jordi S, Yakusheva V, Braccini S, et al. Production and separation of ^{43}Sc for radiopharmaceutical purposes. *EJNMMI Radiopharm Chem*. (2017) **2**:14. doi: 10.1186/s41181-017-0033-9
21. Filosofov D, Loktionova N, Rösch F. A ^{44}Ti/^{44}Sc radionuclide generator for potential application of ^{44}Sc-based PET-radiopharmaceuticals. *Radiochim Acta*. (2010) **98**:149–56. doi: 10.1524/ract.2010.1701
22. Rösch F, Baum RP. Generator-based PET radiopharmaceuticals for molecular imaging of tumours: on the way to THERANOSTICS. *Dalton Trans*. (2011) **40**:6104–11. doi: 10.1039/c0dt01504k
23. Krajewski S, Cydzik I, Abbas K, Bulgheroni A, Simonelli F, Holzwarth U, et al. Cyclotron production of ^{44}Sc for clinical application. *Radiochim Acta*. (2013) **101**:333–8. doi: 10.1524/ract.2013.2032
24. Severin G, Engle J, Valdovinos H, Barnhart T, Nickles R. Cyclotron produced ^{44g}Sc from natural calcium. *Appl Radiat Isotopes*. (2012) **70**:1526–30. doi: 10.1016/j.apradiso.2012.04.030
25. van der Meulen NP, Bunka M, Domnanich KA, Müller C, Haller S, Vermeulen C, et al. Cyclotron production of ^{44}Sc: from bench to bedside. *Nucl Med Biol*. (2015) **42**:745–51. doi: 10.1016/j.nucmedbio.2015.05.005
26. Singh A, van der Meulen NP, Müller C, Klette I, Kulkarni HR, Türler A, et al. First-in-human PET/CT imaging of metastatic neuroendocrine neoplasms with cyclotron-produced ^{44}Sc-DOTATOC: a proof-of-concept study. *Cancer Biother Radiopharm*. (2017) **32**:124–32. doi: 10.1089/cbr.2016.2173
27. Eppard E, de la Fuente A, Benešová M, Khawar A, Bundschuh RA, Gärtner FC, et al. Clinical translation and first in-human use of [^{44}Sc] Sc-PSMA-617 for PET imaging of metastasized castrate-resistant prostate cancer. *Theranostics*. (2017) **7**:4359. doi: 10.7150/thno.20586
28. Armstrong IS, Memmott MJ, Tonge CM, Arumugam P. The impact of prompt gamma compensation on myocardial blood flow measurements with rubidium-82 dynamic PET. *J Nucl Cardiol*. (2018) **25**:596–605. doi: 10.1007/s12350-016-0583-3
29. Lubberink M, Herzog H. Quantitative imaging of 124 I and 86 Y with PET. *Eur J Nucl Med Mol Imaging*. (2011) **38**:10. doi: 10.1007/s00259-011-1768-2
30. Jakoby B, Bercier Y, Conti M, Casey M, Bendriem B, Townsend D. Physical and clinical performance of the mCT time-of-flight PET/CT scanner. *Phys Med Biol*. (2011) **56**:2375. doi: 10.1088/0031-9155/56/8/004
31. Gnesin S, Kieffer C, Zeimpekis K, Papazyan J-P, Guignard R, Prior J, et al. Phantom-based image quality assessment of clinical ^{18}F-FDG protocols in digital PET/CT and comparison with conventional PMT-based PET/CT devices. *EJNMMI Phys*. (2020) 7:1. doi: 10.1186/s40658-019-0269-4
32. Boellaard R, Willemsen A, Arends B, Visser E. *EARL Procedure for Assessing PET/CT System Specific Patient FDG Activity Preparations for Quantitative FDG PET/CT Studies*. (2014). Available online at: http://earl.eanm.org/html/img/pool/EARL-procedure-for-optimizing-FDG-activity-for-quantitative-FDG-PET-studies_version_1_1.pdf (accessed October 23, 2019).
33. Graham MM, Wahl RL, Hoffman JM, Yap JT, Sunderland JJ, Boellaard R, et al. Summary of the UPICT protocol for ^{18}F-FDG PET/CT imaging in oncology clinical trials. *J Nucl Med*. (2015) **56**:955–61. doi: 10.2967/jnumed.115.158402
34. Kaalep A, Sera T, Rijnsdorp S, Yaqub M, Talsma A, Lodge MA, et al. Feasibility of state of the art PET/CT systems performance harmonisation. *Eur J Nucl Med Mol Imaging*. (2018) **45**:1344–61. doi: 10.1007/s00259-018-3977-4
35. Boellaard R, Delgado-Bolton R, Oyen WJ, Giammarile F, Tatsch K, Eschner W, et al. FDG PET/CT: EANM procedure guidelines for tumour imaging: version 2.0. *Eur J Nucl Med Mol Imaging*. (2015) **42**:328–54. doi: 10.1007/s00259-014-2961-x
36. Boellaard R. *EARL: Accreditation Specifications*. (2017). Available online at:http://www.earl.eanm.org/cms/website.php?id=/en/projects/fdg_pet_ct_accreditation/accreditation_specifications.htm (accessed September 9, 2019).

37. Watson CC, Casey ME, Michel C, Bendriem B. Advances in scatter correction for 3D PET/CT. In: *IEEE Symposium Conference Record Nuclear Science,* Vol. 5. Rome (2004). p. 3008–12. doi: 10.1109/NSSMIC.2004.1466317
38. Hayden CH, Casey ME, Watson CC. *Prompt Gamma Correction for Non-Standard Isotopes in a Pet Scanner.* U.S. Patent No. 20080283758A1 (2008). Available online at: https://patents.google.com/patent/US20080283758
39. Zaidi H, Koral KF. Scatter modelling and compensation in emission tomography. *Eur J Nucl Med Mol Imaging*. (2004) **31**:761–82. doi: 10.1007/s00259-004-1495-z
40. van Sluis J, de Jong J, Schaar J, Noordzij W, van Snick P, Dierckx R, et al. Performance characteristics of the digital Biograph Vision PET/CT system. *J Nucl Med*. (2019) **60**:1031–6. doi: 10.2967/jnumed.118.215418
41. Huizing DM, Koopman D, van Dalen JA, Gotthardt M, Boellaard R, Sera T, et al. Multicentre quantitative ^{68}Ga PET/CT performance harmonisation. *EJNMMI Phys*. (2019) **6**:19. doi: 10.1186/s40658-019-0253-z
42. Rosar F, Buchholz HG, Michels S, Hoffmann MA, Piel M, Waldmann CM, et al. Image quality analysis of ^{44}Sc on two preclinical PET scanners: a comparison to ^{68}Ga. *EJNMMI Phys*. (2020) **7**:1–17. doi: 10.1186/s40658-020-0286-3

Conflict of Interest: The authors declare that the research was conducted in the absence of any commercial or financial relationships that could be construed as a potential conflict of interest.